2025 IEEE World Haptics Conference (WHC)
Suwon Convention Center, Suwon, Korea
July 8 ~ 11, 2025

flatLoop: Low-profile Active Force Feedback Device Using Traveling Waves

Zhaochong Cai*
Delft University of Technology
Delft, the Netherlands
z.cai-1@tudelft.nl

Koen Renkema*
ElaadNL
Arnhem, the Netherlands
koen.renkema@gmail.com

Michaël Wiertlewski
Delft University of Technology
Delft, the Netherlands
m.wiertlewski@tudelft.nl

***Abstract*—Active surface haptic devices can guide users by pushing and pulling their fingers. These devices generate active forces directly on the fingertip using resonant traveling waves. Modulating the amplitude of the wave and its direction allows fine control over the force applied to the fingertip, which in turn can be used to create compelling tactile sensations such as elastic potential fields that attract or repel the finger and emulate the feel of curved surfaces. However, existing designs are bulky, with ring-shaped cavities unsuitable for thin consumer electronics. This paper introduces flatLoop, a compact surface haptic device with a height of just 5 mm. It uses a planar aluminum structure with two straight and two curved beams along which flexural waves travel. The thickness of the curved beams varies, steering the wave propagation around corners. Experimental results demonstrate that flatLoop generates uniform traveling waves and produces lateral forces of up to 0.3 N on an 80 × 30 mm² flat surface. This innovative design can deliver rich tactile effects in a compact form, ideal for applications like rendering a flat keyboard where users can feel the shape of keys. This design can facilitate the integration of technology into consumer electronics.**

***Index Terms*—Surface haptics, active force feedback, ultrasonic vibration, traveling waves**

I. Introduction

Since the adoption of touchpads and touchscreens in consumer-electronics, there has been a drive to provide realistic haptic feedback on flat surfaces. While vibrotactile devices are the leading approach, surface haptics has been gaining popularity because these devices let users feel rich tactile feedback during bare finger interactions by modulating the interaction force. The force modulation is typically achieved by varying the friction force via ultrasonic bending waves [1], [2] or electroadhesive attraction [3], [4], enabling the creation of shape illusions [5] or frictional textures for guiding users to specific targets [6], [7]. However, while changing friction produces a salient sensation, it is only effective when the finger is sliding on the surface and little tactile sensation can be created on static fingers. Moreover, because the feedback is passive, the modulated force is always collinear with the direction of movement, and thus not able to effectively guide the user to an arbitrary target. These limitations have been overcome by a new class of surface haptic devices generating *active lateral forces* on sliding or stationary fingers. With active forces, users can be attracted or repelled from specific points. By modulating the force according to finger position or velocity, active force feedback provides tactile guidance or rendering, including navigation through directional cues [8], contour following [9], simulation of button clicks [10]–[12], or creating ”potential fields” on a surface [13]–[15].

Several techniques can generate active forces. The oldest uses asymmetric friction, where the friction of a laterally oscillating surface is changed synchronously to induce a high friction state when the plate moves forward and a low friction state when it moves back [9], [14], [16], [17]. While effective, these systems are often noisy [9], [16] and complex to control [14], [17]. A more recent approach uses ultrasonic flexural traveling waves. When the beam is excited by flexural waves, the surface of the beam follows an elliptical trajectory. This elliptical motion is non-linearly interacting with any object in contact, including skin, creating a net force. The active force is however noticeable only if the wave has a large enough amplitude, on the micrometer scale. To create traveling waves with sufficient amplitude, one can use powerful actuators to vibrate the beam, but the method achieves a small amplitude-to-input power ratio, with energy efficiency often below 1% [18]. Instead, it is possible to use resonance to produce traveling waves. To achieve resonance, we can remember that every traveling wave can be decomposed into two standing waves with a quarter wavelength shift. If these standing waves can be made resonant at the same frequency, they form frequency-degenerate modes and produce a resonating traveling wave with a large amplitude compared to the input; for example, circular-ring traveling-wave ultrasonic motors can reach around 30% energy conversion efficiency [19]. A circular ring used in traveling-wave ultrasonic motors [20], has been used to produce strong active forces on human fingertips [21] and deliver haptic effects such as button clicks [22]. However, their hollow and non-flat shapes are not suitable for touch applications. Another type of structure involves an oblong ring-shaped cavity, as used in a haptic device, the Ultraloop [10]. This structure consists of two straight beams and two semicircular beams, allowing bending waves to propagate along its centerline. The Ultraloop can generate uniform lateral forces on a flat surface and produce tactile effects such as button clicks [10], 3D shapes [15] and viscous damping [23].

Despite its advantages, the Ultraloop is cumbersome. Its height is twice the radius ($2R$), or 100 mm in its current

*Authors ZC and KR contributed equally to this work.
The work of ZC was supported by China Scholarship Council.

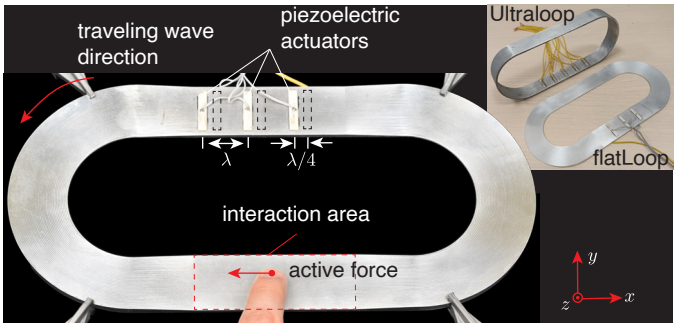

Fig. 1. The flatLoop is a low-profile haptic display that uses flexural traveling waves to provide active force feedback on a bare finger. The inset illustrates a comparison of the dimensions between the Ultraloop and the flatLoop.

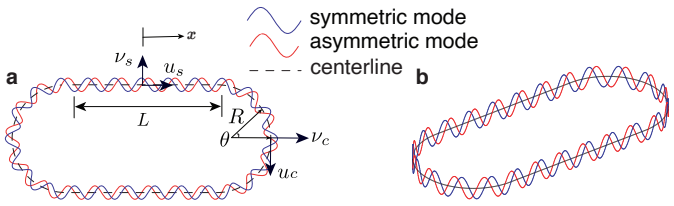

Fig. 2. (a) The oblong centerline of the Ultraloop has two orthogonal degenerate modes of the 24$^{\text{th}}$ order. (b) The flatLoop uses the same centerline as the Ultraloop but features transverse vibrations orthogonal to the centerline's plane.

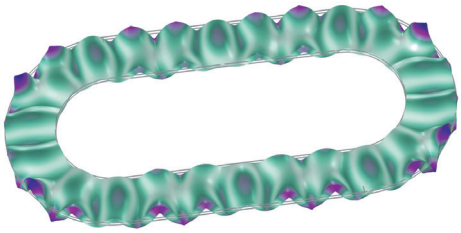

Fig. 3. FEM simulation of the 24$^{\text{th}}$ bending mode shape of the flatLoop with a uniform thickness of 2.75 mm. The difference in the curve length results in 26 wavelengths along the outer circumference and 22 wavelengths along the inner circumference.

configuration. While reducing the radius R could lower the height, the intrinsic $2R$ dimension remains significant, making it ill-suited for integration into most touch-enabled devices, such as touchpads, car dashboards, and display screens in educational or museum settings, which are flat and thin.

In this work, we propose a low-profile design, the flatLoop (Fig. 1), which can support degenerate modes on a flat configuration, reducing the height of the device to that of the thickness of the beam. The design uses the same modes along the centerline as the Ultraloop. However, the planar arrangement includes two curved parts, similar to a running track. These curved parts introduce distortions in the bending wave propagation since the inside of the curve is shorter than its outside. Consequently, to have the same number of wavelengths, the speed of the wave should be higher in the outside. Failing to take the difference in length into account causes the nodal lines in the straight part to be tilted and force generation becomes non-uniform. To address this issue, we employ a variable thickness profile at the curved parts where the thickness follows a power-law function of the radius. This design leads to collinear propagation of the traveling waves in the straight part and uniform force generation. We show how this device can be used by demonstrating a proof-of-concept haptic keyboard, showcasing the potential of the flatLoop for practical applications in touch-based interfaces.

II. Low-Profile Design of a Traveling Wave Structure

A. Orthogonal Degenerate Modes

Previous devices used an oblong ring-type structure excited by two orthogonal modes at the same frequency to create a flexural traveling wave [10], [24]. This type of structure, formed by two straight beams of length L connected by two semicircular segments with a radius R, can be used as a surface haptic device, such as the Ultraloop [10] , or as an acoustic levitation transportation system [24]. To achieve a sufficient amplitude with regular piezoelectric elements, this structure leverages resonance of both modes having an identical resonant frequency. Such distinct vibration modes that share an identical resonant frequency are known as *degenerate modes*. This condition of degeneracy arises only for specific length-to-radius (L/R) ratios. The geometrical criteria for achieving such frequency degeneracy have been discussed in [10], [25], [26]. The flatLoop design revolves around the same oblong centerline loop as our original Ultraloop. Below, we briefly review the analytical model for finding resonances and mode shapes with a given oblong structure.

We define a Cartesian coordinate system and a polar coordinate system for the straight and curved sections respectively (Fig. 2a). The transverse displacements of the straight and curved parts are denoted as ν_s and ν_c . We assume that the form of displacements can be separated into a spatial component (i.e. the mode shape), which depends on coordinate x and θ, and a harmonic component of time t. Thus displacements are expressed as $\nu_s(x,t) = V_s(x)\sin(\omega t)$ and $\nu_c(\theta,t) = V_c(\theta)\sin(\omega t)$, where ω is the angular frequency.

We now consider bending modes with trigonometric forms, i.e. $\pm\sin$ and $\pm\cos$ along the centerline, and are expressed as:

- Symmetric mode: $\{V_s, V_c\} = \{A_s \cos k_s x, A_c \cos k_c\theta\}$
- Asymmetric mode: $\{V_s, V_c\} = \{A_s \sin k_s x, A_c \sin k_c\theta\}$

where k_s is the wave number (with unit in meters) for the straight parts and k_c is the wave number (with units in radians) for the curved parts, and A_s and A_c are the amplitudes of the transverse displacements in the straight and curved parts respectively.

Using the Euler-Bernoulli beam assumption and Hamilton's principle, the dispersion relations coupling k_s, k_c , and ω are derived as follows:

$$k_s^4 - \alpha_s k_s^2\omega^2 - \gamma_s\omega^2 = 0 \tag{1}$$

$$\omega^2(\gamma_c k_c^4 - 2\gamma_c k_c^2 + \alpha_c k_c^2 + \alpha_c + \gamma_c) - k_c^6 + 2k_c^4 - k_c^2 = 0 \tag{2}$$

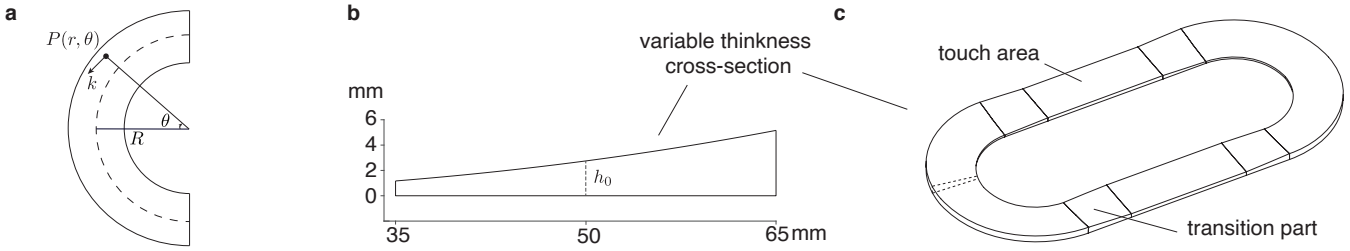

Fig. 4. (a) Top view of the curved segment. (b) Cross-section of the curved bend with variable thickness. (c) The flatLoop design includes two straight beams as the touch surface, two curved bends with variable thicknesses, and four transition sections connecting the curved bends to the straight beams.

where $\alpha_s = \rho/E$, $\gamma_s = (\rho A)/(EI)$, $\alpha_c = (\rho A R^4)/(EI)$ and $\gamma_c = (\rho R^2)/E$. Here, ρ is the material density, E is the Young's modulus, A is the cross-sectional area, and I is the second moment of area.

For the symmetric mode, the boundary conditions ensuring continuity of displacement and rotation between the straight and curved segments are:

$$A_s \cos\left(k_s \frac{L}{2}\right) = A_c \cos\left(-k_c \frac{\pi}{2}\right) \tag{3}$$

$$-A_s k_s \sin\left(k_s \frac{L}{2}\right) = -\frac{A_c k_c}{R} \sin\left(-k_c \frac{\pi}{2}\right) \tag{4}$$

Now Eq. 1, 2, 3, and 4 form a set of coupled equations with four unknowns k_s, k_c, ω and the amplitude ratio $\Gamma = A_s/A_c$. These unknowns, which fully define the symmetric mode shape, can be solved numerically for any given geometry (defined by L, R and h). Similarly, the asymmetric mode shape can be solved using its boundary conditions.

Only at specific discrete L/R ratios, the natural frequencies of symmetric and asymmetric modes coincide. By plotting the $\omega_{sym.}$ and $\omega_{asym.}$ as functions of L/R, configurations with degenerate modes can be identified at their intersection points.

B. Variable Thickness Design

The flatLoop adopts the same oblong centerline as the Ultraloop, with the length L being 140 mm and the radius R being 50 mm. Reusing the configuration of this L and R ensures that all the degenerate modes found valid for the Ultraloop are also present in the flatLoop. However, unlike the Ultraloop (Fig. 2a), the flexural waves in flatLoop are orthogonal to the plane of the centerline (Fig. 2b), creating a planar structure excited by flexural waves. A crude solution to the design of the flatLoop is expanding the oblong centerline in the x-y plane by 30 mm and then extruding the planar shape by 2.75 mm, which matches the width and thickness of the Ultraloop, respectively. However, this uniform-thickness design introduces disparities in the lengths of the wave paths along the inner and outer bends of the curved segments. As shown by finite element method (FEM) simulations in an eigenfrequency study using COMSOL Multiphysics (Fig. 3), the outer bend accommodates more waves than the inner bend. This discrepancy results in tilted nodal lines in straight sections, which challenges the placement of piezoelectric actuators and the uniformity of force generation.

To address this issue, we explored how a variable thickness profile for the curved segments can modulate the wave speed and ultimately achieve aligned nodal lines in the straight part. The idea of the design is to make the flexural waves along the inner and outer bends arrive simultaneously at the end of the curved segment. As illustrated in Fig. 4a, for a point $P(r,\theta)$ in polar coordinates on the curved segment, the wave equality condition means the number of waves along different paths in the curved bend should be constant, expressed as $\pi r k = C_1$, where k is the local wavenumber at the point P with a local thickness h, and C_1 is a constant. The local wavenumber k is determined by the geometry and material properties, and can be approximated using the dispersion equation from Euler-Bernoulli beam theory:

$$k^4 = \omega^2 \frac{\rho A}{EI} \tag{5}$$

Considering a rectangular cross-section, $I = bh^3/12$ and $A = bh$, and substituting these expressions into the equation gives:

$$k^4 = \omega^2 \frac{12\rho}{Eh^2} \tag{6}$$

Assuming ω, E, and ρ are invariant, substituting Eq. 6 into the condition for wave equality gives

$$\frac{h}{r^2} = C_2 \tag{7}$$

Assuming the thickness in the centerline of the curved segments is h_0, we have $C_2 = h_0/R^2$. This yields a quadratic thickness profile for the curved segment (Fig. 4b)

$$h(r) = h_0 (\frac{r}{R})^2 \tag{8}$$

To connect the variable thickness curved bend to the uniform thickness straight part, we use a 30-mm long transition part to linearly transfer the cross-sections (Fig. 4c). FEM simulations were performed to evaluate this design. We observed that the outer bend still had more waves than the inner bend (Fig. 5b), indicating that the quadratic profile was insufficient to fully equalize the wave numbers. This discrepancy is likely due to approximations in the dispersion equation Eq. 5.

To address this, the quadratic thickness equation was modified to include a variable power m:

$$h(r) = h_0 \left(\frac{r}{R}\right)^m \tag{9}$$

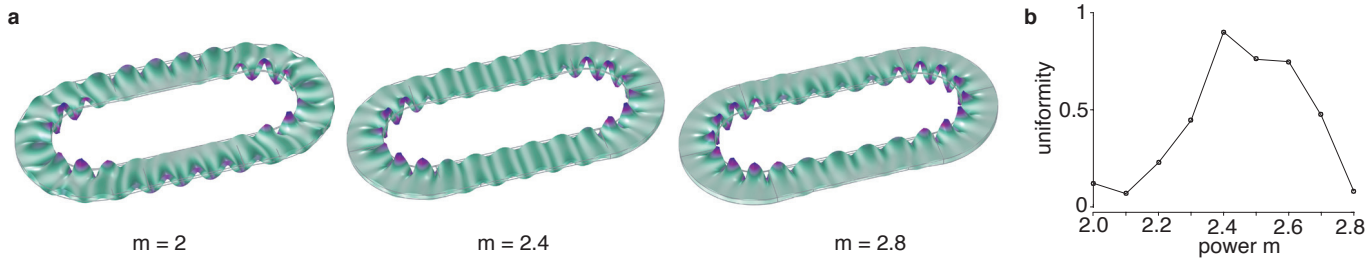

Fig. 5. (a) FEM simulation of the 24th bending mode shape of the flatLoop with a power-law thickness profile in the bends, $h_0(\frac{r}{R})^m$, where m = 2, 2.4, and 2.8. For m = 2, the outer circumference exhibits more wavelengths than the inner circumference. Conversely, for m = 2.8, the outer circumference has fewer wavelengths. For $m = 2.4$, waves are distributed evenly in the straight parts. (b) Uniformity of wave distribution in the straight parts as a function of the power m.

We explored the effect of the power m using FEM to conduct an eigen-frequency study in which the power m ranged from $2.0 \leq m \leq 2.8$ with steps of 0.1. The uniformity in the mode shape, defined as the ratio between the minimum amplitude and the maximum amplitude along the antinodal lines in the straight parts, was evaluated as a function of m, as shown in Fig. 5a. The value of m = 2.4 was found to equalize the number of waves across the curved segments and produce parallel nodal lines on the straight segments (Fig. 5b). This optimized thickness profile was subsequently selected for the physical prototype.

C. Manufacturing and Validation of the Mode Shapes

The flatLoop was fabricated from aluminum 5052 (E = 69 GPa and ρ = 2680 kg/m^3) using CNC machining. Six piezoceramic plates (SMPL25W5T30311, Steiner & Martins Inc.), measuring 25×5×0.3 mm, were glued to one of the straight section of the flatLoop using epoxy adhesive (DP490, 3M). They were arranged in two sets of three: one set on the top surface and the other on the bottom. The piezoceramic elements were spaced one wavelength apart within each set, with the two sets offset by one-quarter wavelength. Each set was connected to an ultrasonic signal source, amplified by a 20× amplifier (PD200, PiezoDrive Inc.). The opposite side of the loop is used as the touch surface, providing a flat interaction area of 80×30 mm^2.

To validate our design, we measured the vibration using a laser Doppler vibrometer (OFV-503 and OFV-5000, Polytec) with a custom scanning attachment. The frequency response of the symmetric and asymmetric modes were obtained by scanning the frequency around the resonance and measuring vibrations at the antinodes of each mode. The frequency sweep signal was generated by a data acquisition board (USB-6351, National Instruments). The resonant frequencies of the two degenerate modes were closely spaced at 38,601 Hz and 38,596 Hz, as shown in Fig. 6a. Because both modes are close, we set the working frequency as the average which was sufficient to excite traveling waves with a high vibration amplitude.

The symmetric and asymmetric mode shapes were further characterized by scanning the 80×30 mm^2 touch surface with an 1×1 mm^2 grid. These mode shapes were orthogonal (Fig. 6b and c), although some modal lines appeared distorted. These distortions may be attributed to manufacturing imperfections or the influence of transition parts, which requires further investigation.

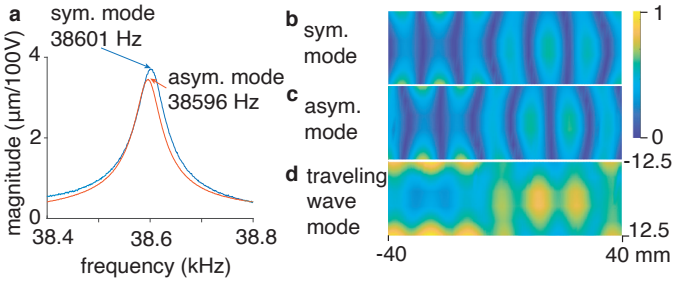

Fig. 6. (a) Experimental frequency response of the two frequency-degenerate modes. (b) Normalized colormaps of the mode shapes of symmetric mode, asymmetric mode, and the resulting traveling wave mode.

A traveling wave pattern can be observed by superimposing these two degenerate modes with a 90-degree temporal phase shift, see Fig. 6d, although several nodal regions are still visible.

III. Characterization of Force Generation

The main performance metric of these devices is how salient the sensation is. To quantify the saliency, which is linked to the strength of the stimulus, we measured the net lateral force on a stationary human finger under varying normal forces and phase shifts. Additional measurements were conducted on a sliding finger to evaluate force behavior during dynamic interaction.

A. Force Measurement Setup and Force Generation

The flatLoop was supported by four 3D printed PLA fixtures attached to its curved segments. These fixtures were mounted on a 250 mm×70 mm PMMA plate, which was fastened to a 6-axis force/torque sensor (HEX32, ReSense). A 3D-printed finger holder fixed to a grounded structure constrained the finger movement in the lateral direction, similar to the one used in [10]. This setup enabled the force sensor to measure the net lateral force exerted on the stationary finger.

During the measurements, the experimenter placed his index finger in the holder and maintained a normal force of approximately 1 N with visual feedback from real-time force value. The phase shift of the driving signal was then

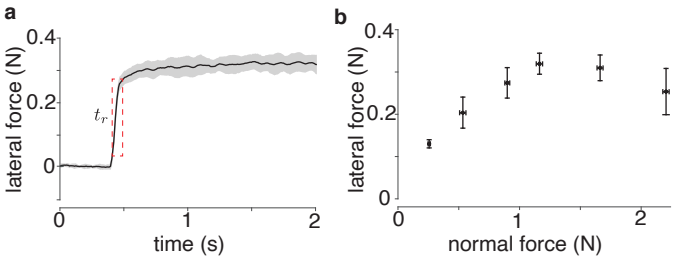

Fig. 7. (a) Net lateral force measured at x = 30 mm on a stationary finger when the phase shift was abruptly switched from 0° to 90 °. The curves are aligned to the moment of phase switching. The rise time t_r = 0.12 s. The shaded area represents the standard deviation. (b) Net lateral force as a function of the normal force.

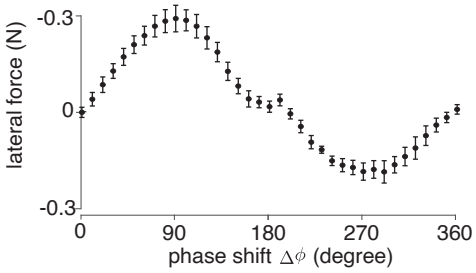

Fig. 8. Lateral force as a function of phase shift $\Delta\phi$ with each condition repeated nine times. Error bars represent the standard deviation.

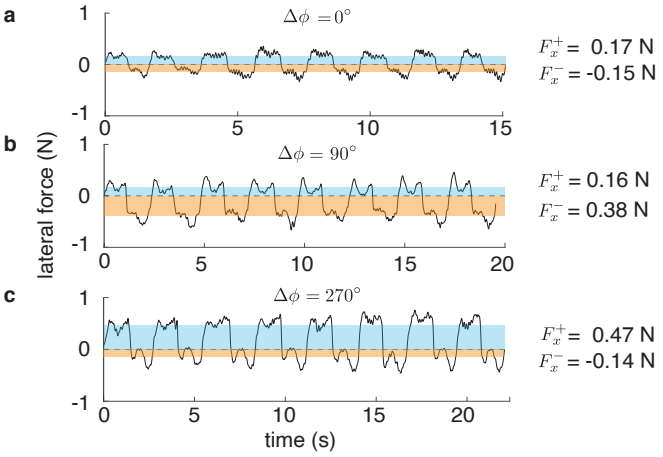

Fig. 9. Symmetric resistance was observed in (a) under a standing wave condition. In contrast, in (b) and (c), higher resistance is observed when the finger slides against the particle motion, compared to when the finger slides in the direction of particle motions. The shaded areas represent the average positive (blue) and negative (orange) forces.

abruptly switched from 0° to 90°, while the voltage sent to the piezoelectric actuators remained constant at ±3 V × 20. This driving voltage produced a vibration amplitude of ± 2.3 µm for traveling waves when there is no finger in contact. The net lateral force was calculated as the change in force when the phase shift was switched to 90°. The averaged lateral force across 18 trials was measured as 0.31 N (Fig. 7a).

B. Lateral Force versus Normal Force

To study the effect of normal force on the lateral force generation, we measured the lateral force under varying normal forces of 0.2, 0.5, 0.9, 1.1, 1.6, and 2.2 N at x = 30 mm on the touch surface. Each normal force condition was tested in three trials, with each trial comprising eight times of phase switches from 0° to 90°. As shown in Fig. 7b, the lateral force increased approximately linearly with normal force for $F_N \leq$ 1.1 N. However, at higher normal forces (F_N = 1.6 N and 2.2 N), the lateral force decreased, which is likely due to damped vibrations by the finger. These results suggest that for optimal tactile feedback on traveling wave devices, the applied normal force should remain within an appropriate range, ideally not exceeding 1 N, and these devices should also compensate for the damped vibrations to provide a stable force generation.

C. Lateral Force versus Phase Shift

The lateral force at x = 30 mm was measured under varying phase shifts between two standing waves, with the normal force maintained at 1 N. Each phase shift in the range of 0° to 360° with an increment of 10° was measured nine times. As shown in Fig. 8, the lateral force exhibits a sinusoidal relationship with phase shift, reaching a maximum rightward force of 0.3 N at 90° and a maximum leftward force of 0.2 N at 270°. The lateral force was near zero at 0° and 180°. This sinusoidal force-phase trend is consistent with previous observations on the Ultraloop. The observed asymmetry between force magnitudes at 90° and 270° may result from the non-uniform mode shape at these phase shifts, as seen in Fig. 6b.

D. Lateral Force versus Sliding Direction

Lateral force generation is typically evaluated on a stationary fingertip. However, sliding gestures are common in touchpad or touchscreen interactions. In this experiment, we measured the lateral force when a finger is sliding in and against the traveling wave direction. After training, the experimenter could slide the index finger back and forth at a relatively constant speed while maintaining a normal force of ≈1 N. The sliding was repeated eight times. The phase conditions in these trials were 0°, 90° or 270°.

At a 0° phase shift, the flatLoop generates standing waves. The lateral force was roughly symmetric between both sliding directions, with the average positive force being 0.17 N, and the average negative force being 0.15 N, see Fig. 9a. This symmetry indicates that no net lateral force was produced under these conditions. Instead, the fingertip experienced only sliding friction opposing the motion.

At a 90° phase shift, where the traveling waves propagate clockwise, the surface generates rightward lateral forces on a stationary finger. However, when the finger is sliding, it encounters resistance in both sliding directions, as shown in Fig. 9b. Notably, when sliding against the net force direction, a higher resistance force is observed, with an average force of 0.38 N compared to 0.165 N when sliding back. Similarly, at a 270° phase shift, the observed asymmetry reversed (Fig. 9c). These observations suggest that the active lateral forces might

only generate a ”pushing” effect on a static or a slow-moving finger. When a finger slides in the direction of the surface particle motion but at a speed exceeding the particle velocity, the global force is still resistive and not propulsive, contrary to the behavior observed with a static finger.

IV. Demonstration: A Haptic Keyboard

Active haptic devices can effectively provide force feedback on users and can be used to construct artificial potential fields or guide users' limb in virtual or remote environments [27], [28]. However, the application of potential field rendering for fingertip guidance remains limited in human-computer interaction applications [9]. Here, we designed a haptic keyboard application using the flatLoop to demonstrate the practicality of our device in real-world scenarios. The haptic keyboard aims to restore the tangibility of physical keys by generating attractive potential wells aligned with the keyboard layout. Fig. 10a illustrates the interactive user interface displayed on a screen, programmed by Python, which consists of three rows of keys arranged in the standard ”QWERTY” configuration. Each key is represented by an individual Gaussian potential well, and the corresponding local force field is derived as the negative gradient of the potential field (Fig. 10b). As a user's finger slides over the touch surface, a position sensor (Neonode, NNAMC1580PCEV) located above the surface tracks the finger's x and y coordinates. The position data is transmitted to a microcontroller (Teensy 3.6), which modulates the amplitude and phase of the ultrasonic driving signals to produce the desired lateral forces. These potential fields could help users to navigate over the keys, enabling faster and easier typing.

To evaluate the system, we recorded the lateral forces generated as a finger slid across the center row of the keyboard 6 times. Fig. 10c shows the measured force as a function of position. The integration of the averaged force curve reveals distinct potential wells aligned with keys ”F,” ”G,” and ”H” (Fig. 10c), aligning with the proposed tactile experience.

V. Discussions and Conclusions

We designed a low-profile active surface haptic device that uses resonant traveling waves. The cross-section follows a power-law with a power of 2.4, which was determined by analytical model and FEM simulations, leading to even wave distribution. Our design achieves comparable performance to the original device, the Ultraloop, while significantly reducing its height. The flatLoop generated $3.58\,\mu\mathrm{m}/100$ V versus $3.73\,\mu\mathrm{m}$ /100 V in the Ultraloop, and a maximum force of 0.31 N vs. 0.3 N when the normal force is 1 N. The current design reduces the height from 100 mm to 5 mm by using a planar configuration, as seen by a side-by-side comparison of dimensions in the inset in Fig. 1.

One limitation of the prototype is that the observed nodal lines in the straight parts are not fully parallel compared to FEM simulations, resulting in less uniform wave distribution and uneven force production. This discrepancy may arise from imprecision in the CNC machining process, mechanical

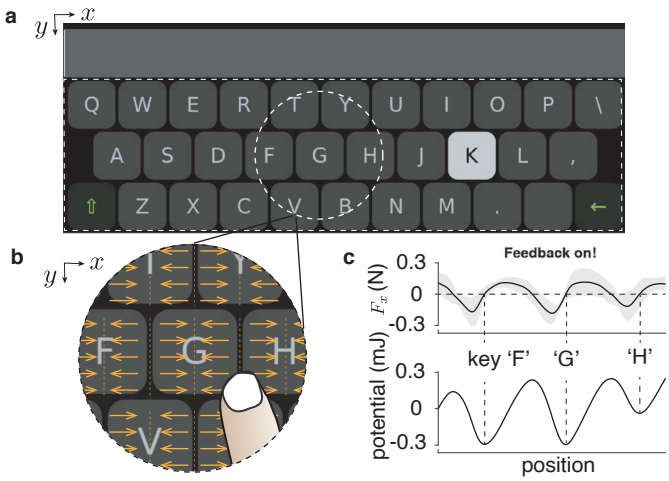

Fig. 10. Demonstration of a haptic keyboard. (a) The user interface displayed on an external screen. Users can interact with the interface by sliding on the flatLoop. (b) Visualization of the desired force fields within the dashed circle. (c) The lateral force measured on a slowly sliding finger across the centerline in the dashed circle area. The graph below shows the calculated potential values derived as the integral of the lateral force. The shaded area represents the standard deviation.

interference introduced by the added piezoceramic plates, or the potential suboptimal selection of m = 2.4 based on FEM results. Refining the mode shape through further investigation of the power parameter of m may improve uniformity. Additionally, the effect of uneven force production can be mitigated in real applications by tuning the actuation level to normalize local vibration amplitudes.

Another limitation is the absence of an explicit force production model that accounts for sliding velocity and the geometry of the elliptical trajectory. Our experiments measured the forces during sliding against and along the wave propagation direction. The variation in force of these two cases supports the model proposed by Ghenna et al., who measured the lateral force in a surface haptic device with elliptical surface motions [8]. Future studies should investigate force production as a function of sliding velocity and the potential field rendering can consider the velocity as an input, which currently depends solely on position.

In conclusion, we introduced the flatLoop, a low-profile active force feedback device with a height of 5 mm, designed for potential field rendering. The flatLoop features a touch surface of 80×30 mm^2 and generates a maximum lateral force of 0.31 N, comparable to the Ultraloop while offering improved usability due to its compact size. This innovation makes it suitable for integration into devices such as information terminals and car dashboards. Future work should focus on modeling and optimizing the transition region to further increase the area of the touch surface and conducting user studies to evaluate 2D potential field rendering.

References

[1] L. Winfield, J. Glassmire, J. E. Colgate, and M. Peshkin, “T-pad: Tactile pattern display through variable friction reduction,” in *Second Joint EuroHaptics Conference and Symposium on Haptic Interfaces for Virtual*

Environment and Teleoperator Systems (WHC'07). IEEE, 2007, pp. 421–426.

[2] M. Wiertlewski, R. Fenton Friesen, and J. E. Colgate, "Partial squeeze film levitation modulates fingertip friction," *Proceedings of the National Academy of Sciences*, vol. 113, no. 33, pp. 9210–9215, 2016.

[3] O. Bau, I. Poupyrev, A. Israr, and C. Harrison, "Teslatouch: electrovibration for touch surfaces," in *Proceedings of the 23nd Annual ACM Symposium on User Interface Software and Technology*, 2010, pp. 283–292.

[4] M. Ayyildiz, M. Scaraggi, O. Sirin, C. Basdogan, and B. N. Persson, "Contact mechanics between the human finger and a touchscreen under electroadhesion," *Proceedings of the National Academy of Sciences*, vol. 115, no. 50, pp. 12 668–12 673, 2018.

[5] S.-C. Kim, A. Israr, and I. Poupyrev, "Tactile rendering of 3d features on touch surfaces," in *Proceedings of the 26th Annual ACM Symposium on User Interface Software and Technology*, 2013, pp. 531–538.

[6] V. Levesque, L. Oram, K. MacLean, A. Cockburn, N. D. Marchuk, D. Johnson, J. E. Colgate, and M. A. Peshkin, "Enhancing physicality in touch interaction with programmable friction," in *Proceedings of the SIGCHI Conference on Human Factors in Computing Systems*, 2011, pp. 2481–2490.

[7] C. Bernard, J. Monnoyer, S. Ystad, and M. Wiertlewski, "Eyes-off your fingers: Gradual surface haptic feedback improves eyes-free touchscreen interaction," in *Proceedings of the 2022 CHI Conference on Human Factors in Computing Systems*, 2022, pp. 1–10.

[8] S. Ghenna, E. Vezzoli, C. Giraud-Audine, F. Giraud, M. Amberg, and B. Lemaire-Semail, "Enhancing variable friction tactile display using an ultrasonic travelling wave," *IEEE Transactions on Haptics*, vol. 10, no. 2, pp. 296–301, 2016.

[9] E. C. Chubb, J. E. Colgate, and M. A. Peshkin, "Shiverpad: A glass haptic surface that produces shear force on a bare finger," *IEEE Transactions on Haptics*, vol. 3, no. 3, pp. 189–198, 2010.

[10] Z. Cai and M. Wiertlewski, "Ultraloop: Active lateral force feedback using resonant traveling waves," *IEEE Transactions on Haptics*, vol. 16, no. 4, pp. 652–657, 2023.

[11] H. Xu, R. L. Klatzky, M. A. Peshkin, and J. E. Colgate, "Localizable button click rendering via active lateral force feedback," *IEEE Transactions on Haptics*, vol. 13, no. 3, pp. 552–561, 2020.

[12] P. Garcia, F. Giraud, B. Lemaire-Semail, M. Rupin, and A. Kaci, "Control of an ultrasonic haptic interface for button simulation," *Sensors and Actuators A: Physical*, vol. 342, p. 113624, 2022.

[13] X. Dai, J. E. Colgate, and M. A. Peshkin, "Lateralpad: A surface-haptic device that produces lateral forces on a bare finger," in *2012 IEEE Haptics Symposium (HAPTICS)*. IEEE, 2012, pp. 7–14.

[14] H. Xu, M. A. Peshkin, and J. E. Colgate, "Ultrashiver: Lateral force feedback on a bare fingertip via ultrasonic oscillation and electroadhesion," *IEEE Transactions on Haptics*, vol. 12, no. 4, pp. 497–507, 2019.

[15] Z. Cai, D. Abbink, and M. Wiertlewski, "Attracting fingers with waves: Potential fields using active lateral forces enhance touch interactions," in *Proceedings of the 2025 CHI Conference on Human Factors in Computing Systems*, 2025, pp. 1–13.

[16] J. Mullenbach, M. Peshkin, and J. E. Colgate, "eshiver: Lateral force feedback on fingertips through oscillatory motion of an electroadhesive surface," *IEEE Transactions on Haptics*, vol. 10, no. 3, pp. 358–370, 2016.

[17] H. Xu, M. A. Peshkin, and J. E. Colgate, "Switchpad: Active lateral force feedback over a large area based on switching resonant modes," in *Haptics: Science, Technology, Applications: 12th International Conference, EuroHaptics 2020, Leiden, The Netherlands, September 6–9, 2020, Proceedings 12*. Springer, 2020, pp. 217–225.

[18] M. Kuribayashi, S. Ueha, and E. Mori, "Excitation conditions of flexural traveling waves for a reversible ultrasonic linear motor," *The Journal of the Acoustical Society of America*, vol. 77, no. 4, pp. 1431–1435, 1985.

[19] Shinsei Corporation, "Ultrasonic motor products," https://www.shinsei-motor.com/en/product/standard/index.html, 2025, accessed: 2025-05-10.

[20] C. Zhao, *Ultrasonic motors: technologies and applications*. Springer Science & Business Media, 2011.

[21] M. Biet, F. Giraud, F. Martinot, and B. Semail, "A Piezoelectric Tactile Display Using Travelling Lamb Wave," in *Proceedings of Eurohaptics*, Paris, France, 2006, pp. 567–570.

[22] D. Gueorguiev, A. Kaci, M. Amberg, F. Giraud, and B. Lemaire-Semail, "Travelling ultrasonic wave enhances keyclick sensation," in *Haptics: Science, Technology, and Applications: 11th International Conference, EuroHaptics 2018, Pisa, Italy, June 13-16, 2018, Proceedings, Part II 11*. Springer, 2018, pp. 302–312.

[23] Z. Cai and M. Wiertlewski, "Viscous damping displayed by surface haptics improves touchscreen interactions," in *International Conference on Human Haptic Sensing and Touch Enabled Computer Applications*. Springer, 2024, pp. 352–364.

[24] G. P. Thomas, M. A. Andrade, J. C. Adamowski, and E. C. N. Silva, "Development of an acoustic levitation linear transportation system based on a ring-type structure," *IEEE Transactions on Ultrasonics, Ferroelectrics, and Frequency control*, vol. 64, no. 5, pp. 839–846, 2017.

[25] G. Thomas, C. Kiyono, A. Gay Neto, and E. Silva, "Conceptual design of oblong ring vibrators," *Journal of Vibration and Acoustics*, vol. 142, no. 2, p. 021001, 2020.

[26] X. Liu, D. Shi, Y. Civet, and Y. Perriard, "Modelling and optimal design of a ring-type structure for the generation of a traveling wave," in *2013 International Conference on Electrical Machines and Systems (ICEMS)*. IEEE, 2013, pp. 1286–1291.

[27] J. Ren, K. A. McIsaac, R. V. Patel, and T. M. Peters, "A potential field model using generalized sigmoid functions," *IEEE Transactions on Systems, Man, and Cybernetics, Part B (Cybernetics)*, vol. 37, no. 2, pp. 477–484, 2007.

[28] P. Marayong and A. M. Okamura, "Speed-accuracy characteristics of human-machine cooperative manipulation using virtual fixtures with variable admittance," *Human Factors*, vol. 46, no. 3, pp. 518–532, 2004.